Autonomous GNSS-based Relative Navigation for Distributed Earth Observation Missions using Adaptive Extended Kalman Filter

Alessandro Michelazzi(1), Gabriella Gaias(2), Camilla Colombo(3)

(1) Department of Aerospace Science and Technology, Politecnico di Milano
Milan, Italy
Email: alessandro.michelazzi@polimi.it

(2) Department of Aerospace Science and Technology, Politecnico di Milano
Milan, Italy
Email: gabriella.gaias@polimi.it

(3) Department of Aerospace Science and Technology, Politecnico di Milano
Milan, Italy
Email: camilla.colombo@polimi.it

***Abstract* – This paper investigates the feasibility of GNSS-based relative navigation for close formation flying missions with inter-satellite distances at the metre level. An Extended Kalman Filter (EKF) is developed to process single-frequency multi-constellation GNSS measurements, including GRAPHIC and single-difference carrier-phase combinations, within a multi-satellite architecture where each spacecraft independently estimates the relative states.**

To enhance robustness and enable greater onboard autonomy, an adaptive filtering approach based on the Adaptive Dynamic Model Compensation (ADMC) technique is integrated into the EKF framework. This method enables the online estimation of the process noise associated with unmodelled dynamics while preserving consistency with the underlying dynamical model.

A sensitivity analysis is conducted to assess the impact of key design parameters. Results show that both the baseline EKF and the adaptive formulation achieve millimetre-level relative positioning accuracy under nominal conditions. While the baseline EKF may provide slightly better nominal accuracy under optimal tuning, the adaptive approach exhibits improved robustness to parameter selection and initialisation, supporting enhanced autonomy and reliability for safety-critical missions.

I. INTRODUCTION

Formation flying missions are enabling a new class of space applications requiring high-precision relative navigation between multiple spacecraft. Among the available techniques, GNSS-based solutions have long been a predominant choice for missions involving cooperative satellites in Low Earth Orbit (LEO), as they provide accurate and reliable measurements suitable for onboard real-time applications.

New mission concepts are being investigated for Earth Observation, where satellite formations enable distributed instruments whose performance can surpass that of a single platform. Such applications may require very short inter-satellite baselines, down to the metre level, as in the case of interferometric radiometry [1]. These short distances impose stringent requirements on the knowledge of the relative state, pushing the limits of current state-of-the-art GNSS-based relative navigation algorithms. Moreover, the reduced separation between spacecraft introduces additional challenges in terms of mission safety. In this context, autonomy plays a key role in enhancing mission safety, reducing reliance on ground-based operations. This trend is consistent with the increasing emphasis on autonomous capabilities in modern space missions. Within the navigation domain, such autonomy can be achieved through the use of adaptive filtering techniques, which allow the estimation process to adjust to time-varying uncertainties and modelling errors.

Historically, most formation flying missions have relied on the Extended Kalman Filter (EKF) to process GNSS measurements and provide real-time relative navigation solutions. Representative examples include PRISMA [2], CanX-4/5 [3], TanDEM-X [4]. The main differences among these missions lie in the estimated state parameters and in the type of GNSS observables processed.

Current state-of-the-art techniques for onboard applications have demonstrated unprecedented levels of accuracy. For instance, in [5], relative navigation performance at the sub-centimetre level is achieved.

Adaptive filtering techniques have been widely studied in the literature and have also been applied to GNSS-based EKF frameworks for formation flying. An early example is the work of [6], where covariance matching techniques were applied to formation scenarios with kilometre-scale baselines. Other studies have explored approaches based on Maximum Likelihood Estimation and fuzzy logic to adaptively tune the process and

measurement noise covariance matrices [7], achieving relative navigation accuracy at the decimetre level.
Although not specifically developed for GNSS-based navigation, the work presented in [8] is of particular relevance. In this contribution, State Noise Compensation and Dynamic Model Compensation (DMC) are combined with covariance matching within an adaptive filtering framework. A key advantage of this approach is the explicit incorporation of dynamical model constraints, while avoiding the need for ad hoc methods to ensure that the process noise covariance remains positive semi-definite.

In this context, the present work aims to investigate the applicability of GNSS-based relative navigation to close formation flying missions with very short inter-satellite baselines (below 10 m), with particular emphasis on the achievable navigation accuracy under these conditions. Furthermore, the paper evaluates the potential of adaptive filtering techniques to enhance estimation robustness, increase onboard autonomy, and ultimately contribute to mission safety.
To this end, the adaptive filtering strategy proposed in [8] is adopted and extended to the case of GNSS-based relative navigation in LEO formation flying. In particular, the Adaptive Dynamic Model Compensation (ADMC) approach is integrated within an EKF framework and tailored to account for a multi-satellite system. Its performance is assessed through comparison with a standard EKF formulation, highlighting the benefits and limitations of adaptive filtering in close-proximity scenarios.

Section II presents the baseline EKF, while Section III describes the adaptive filtering approach adopted in this work. Section IV then provides the results, including a sensitivity analysis of key design parameters and a comparison of the final performance of both the baseline and adaptive filters.

II. Baseline Extended Kalman Filter

In order to assess the feasibility of GNSS-based relative navigation for close formation flying, a carefully designed EKF is developed. The filter architecture and modelling choices play a crucial role in determining the achievable accuracy, particularly in scenarios with inter-satellite distances below 10 m.
The EKF presented here is designed for a formation of three satellites. Unlike most formation flying studies, each satellite independently runs its own EKF and produces a relative navigation solution. This design choice is motivated by the critical conditions associated with close formation flying missions, where robustness and fault tolerance are essential for safety. In particular, this distributed architecture ensures that the formation can continue operating even in contingency scenarios, such as the loss of one satellite.

The filter design begins with the definition of the GNSS observables. Following the approach in [5], two types of single-frequency measurement combinations are considered. The first is the GRAPHIC (GRoup And Phase Ionospheric Correction) combination, defined as the average of the pseudorange and carrier-phase measurements. This provides an absolute measurement that eliminates the first-order ionospheric delay, at the cost of introducing a term related to the carrier-phase ambiguity.
The second observable is the Single-Difference Carrier Phase (SDCP), which provides high-accuracy relative measurements. This improved accuracy arises both from the intrinsic precision of carrier-phase observations compared to pseudorange measurements, and from the single-difference formulation, which cancels common errors such as GNSS satellite clock offsets, broadcast ephemeris errors, and signal path delays, given the short inter-satellite separation.
In addition, signals from both the GPS and Galileo constellations are used. This increases the number of visible satellites, thereby improving both the accuracy and robustness of the navigation solution.
The measurement vector is defined as:

$$\boldsymbol{z} = \left[\boldsymbol{z}_{\mathrm{A}}^{\mathrm{GR}}\ \boldsymbol{z}_{\mathrm{B}}^{\mathrm{GR}}\ \boldsymbol{z}_{\mathrm{C}}^{\mathrm{GR}}\ \boldsymbol{z}_{\mathrm{AB}}^{\mathrm{SDCP}}\ \boldsymbol{z}_{\mathrm{AC}}^{\mathrm{SDCP}}\right] \tag{1}$$

where A denotes the satellite on which the filter is running, while B and C represent the other two satellites. This measurement formulation implies that each satellite shares its raw GNSS measurements with the others in the formation, and in turn receives their measurements. In this work, such information exchange is assumed to be instantaneous, which is considered acceptable for this preliminary analysis.

The estimation state vector is defined as:

$$\begin{aligned}\boldsymbol{x} = [\ &\boldsymbol{r}^{\mathrm{A}}\ \boldsymbol{v}^{\mathrm{A}}\ \boldsymbol{a}_{emp}^{\mathrm{A}}\ c\delta t^{\mathrm{A}}\ c\dot{\delta t}^{\mathrm{A}}\ \boldsymbol{N}^{\mathrm{A}} \\ &\boldsymbol{r}^{\mathrm{B}}\ \boldsymbol{v}^{\mathrm{B}}\ \boldsymbol{a}_{emp}^{\mathrm{B}}\ \Delta c\delta t^{\mathrm{AB}}\ \Delta c\dot{\delta t}^{\mathrm{AB}}\ \boldsymbol{N}_{\mathrm{SD}}^{\mathrm{AB}} \\ &\boldsymbol{r}^{\mathrm{C}}\ \boldsymbol{v}^{\mathrm{C}}\ \boldsymbol{a}_{emp}^{\mathrm{C}}\ \Delta c\delta t^{\mathrm{AC}}\ \Delta c\dot{\delta t}^{\mathrm{AC}}\ \boldsymbol{N}_{\mathrm{SD}}^{\mathrm{AC}}]\end{aligned} \tag{2}$$

The state vector includes, for each spacecraft (i.e., i = A, B, C), its inertial position $\boldsymbol{r}^{i}$, velocity $\boldsymbol{v}^{i}$, and a set of empirical accelerations $\boldsymbol{a}_{emp}^{i}$ expressed in the radial-transversal-normal (RTN) frame of satellite i, to account for unmodelled dynamics. For spacecraft A, the filter also estimates its receiver clock bias and drift ($c\delta t^{\mathrm{A}}, c\dot{\delta t}^{A}$) together with the corresponding carrier-phase ambiguity states $\boldsymbol{N}^{A}$. For spacecraft B and C, the clock states are expressed as inter-satellite differences with respect to A, ($\Delta c\delta t^{\mathrm{AB}}$, $\Delta c\dot{\delta t}^{\mathrm{AB}}$) and ($\Delta c\delta t^{\mathrm{AC}}$, $\Delta c\dot{\delta t}^{\mathrm{AC}}$). The ambiguity states correspond to the single-difference carrier-phase ambiguities $\boldsymbol{N}_{\mathrm{SD}}^{\mathrm{AB}}$ and $\boldsymbol{N}_{\mathrm{SD}}^{\mathrm{AC}}$.

The spacecraft positions and velocities are propagated

through numerical integration of the equations of motion and the associated variational equations. In this work, only the perturbation due to the Earth's geopotential is considered, using the GRACE gravity model (GGM01S) up to degree and order 20.
Following the DMC approach, the empirical accelerations are modelled as a first-order Gauss-Markov process [9]:

$$\boldsymbol{a}(t+\Delta t) = e^{-\frac{\Delta t}{\tau}}\boldsymbol{a}(t) + \boldsymbol{w} \tag{3}$$

where $\boldsymbol{w} \sim N\left(0, \frac{q\tau}{2}\left(1 - e^{-\frac{2\Delta t}{\tau}}\right)\right)$, Δt is the time step, $\boldsymbol{\tau}$ is the autocorrelation time, and $\boldsymbol{q}$ is the power spectral density describing the intensity of the random input.
The clock bias and drift are modelled as a two-state random-process [10], while the carrier-phase ambiguities are treated as constants during the prediction step.
Once the filter has converged, the SDCP ambiguities are fixed to integer values using the widely adopted LAMBDA method [11], together with the validation tests proposed in [5]. After ambiguity fixing, the corresponding covariance entries are constrained to zero.

III. ADAPTIVE FORMULATION

In the context of close formation flying, robustness and autonomy are critical requirements for ensuring mission safety. Although the baseline EKF provides accurate estimates under nominal conditions, its performance may be sensitive to variations in measurement quality and, more generally, to unmodelled or time-varying dynamics.
While the present study considers a simplified scenario without manoeuvres, nominal operations may require continuous control to maintain the formation. In such cases, the impact of time-varying dynamics and modelling uncertainties is expected to be even more significant. For this reason, adaptive filtering techniques are introduced to enable the filter to adjust its behaviour in response to changing conditions.

Among the state-of-the-art adaptive techniques, the ADMC approach proposed in [8] is adopted, as it effectively bridges DMC with covariance-matching adaptive filtering. The method enables online estimation of the process noise covariance while preserving consistency with the underlying dynamical model. In contrast to many adaptive approaches, it naturally guarantees a positive semi-definite covariance matrix and remains robust during measurement outages.
The core of the ADMC approach is a constrained weighted least-squares minimisation, used to estimate the process noise covariance at each time step. In practice, this optimisation adjusts the covariance parameters associated with the empirical accelerations so that the theoretical prediction of the state error statistics matches those inferred from the filter residuals. The comparison is performed on the satellite state components, namely absolute position and velocity.
The weighting matrix assigns greater importance to components that are estimated with higher confidence, while the imposed bounds ensure physically meaningful solutions and prevent unrealistic values. As a result, the estimated process noise covariance remains consistent with both the observed filter behaviour and prior knowledge of the dynamical environment.

In this work, the ADMC formulation is tailored to the specific problem of GNSS-based relative navigation in close formation flying. Rather than re-deriving the original method, the focus is placed on its adaptation and integration within the EKF architecture described in the previous section.
A first important aspect concerns the multi-satellite nature of the state. Indeed, the least-squares minimisation is performed independently for each spacecraft in the filter, by considering the corresponding position, velocity, and empirical acceleration states separately. This choice is consistent with the formulation of the empirical process noise covariance, defined as an average over a sliding window of length N computed as:

$$\widehat{\mathbf{Q}}_k = \frac{1}{N}\sum_{p=k-N}^{k-1}\left(\mathbf{P}_{p|p} - \mathbf{\Phi}_p\mathbf{P}_{p-1|p-1}\mathbf{\Phi}_p^T + \mathbf{\Delta}_p^x{\mathbf{\Delta}_p^x}^T\right) \tag{4}$$

where $\mathbf{P}_{i|j}$ denotes the state covariance at time step i after processing measurements at time step j, $\mathbf{\Phi}_i = \mathbf{\Phi}(t_i, t_{i-1})$ is the state transition matrix from time t_{i-1} to t_i and $\mathbf{\Delta}_i^x$ is the state correction obtained during the filter update step. During measurement outages, the corresponding samples are excluded from (4). Since such outages may affect only a subset of the spacecraft, the estimation of the empirical process noise covariance must be carried out independently for each satellite, which naturally leads to a separate least-squares minimisation for each one. The mathematical formulation is:

$$\arg\min_{\boldsymbol{q}} \left(\mathbf{X}_k^m\boldsymbol{q} - \widehat{\boldsymbol{q}}_{s,k}^m\right)^T {\mathbf{W}_k^m}^{-1}\left(\mathbf{X}_k^m\boldsymbol{q} - \widehat{\boldsymbol{q}}_{s,k}^m\right) \tag{5}$$

where $\widehat{\boldsymbol{q}}_{s,k}^m$ denotes the empirical process noise covariance of the state associated with spacecraft m, expressed in vector form, and $\boldsymbol{q}$ is the column vector containing the process noise power spectral densities of the empirical accelerations for spacecraft m.
Following the formulation in [8], the empirical covariance is represented using the half-vectorisation operator, denoted as $\mathrm{vech}(\cdot)$, which stacks the lower triangular elements of a symmetric matrix into a vector.

This allows the least-squares problem to be formulated using only the unique elements of the covariance matrices, thereby reducing the computational burden. Accordingly, $\hat{\boldsymbol{q}}_{s,k}^m = \text{vech}(\hat{\mathbf{Q}}_{s,k}^m)$ with $\hat{\mathbf{Q}}_{s,k}^m$ the submatrix of the empirical process noise covariance associated with the state of satellite m.

The matrix $\mathbf{W}_k^m$ represents the theoretical covariance of $\hat{\boldsymbol{q}}_{s,k}^m$, while $\mathbf{X}_k^m$ maps the vector $\boldsymbol{q}$ to the corresponding state process noise covariance in vectorised form.

Since, in this work, the empirical accelerations are expressed in the RTN frame, the formulation slightly differs from that in [8] due to the inclusion of the appropriate frame rotation. In particular, each column of $\mathbf{X}_k^m$ is computed as:

$$\mathbf{X}_{k,(:,j)}^m = \text{vech}\left(\begin{bmatrix}\gamma_{pp}^m & \gamma_{pv}^m \\ \gamma_{pv}^m & \gamma_{vv}^m\end{bmatrix} \otimes \boldsymbol{r}_j^m \boldsymbol{r}_j^{mT}\right) \quad (6)$$

where γ_{pp} , γ_{pv}, and γ_{vv} are the coefficients defined in [9], and $\boldsymbol{r}_j$ is the j-th column of the rotation matrix from the Earth-Centred Inertial (ECI) frame to the RTN frame of satellite m, assumed constant over each EKF time step.

The optimal solution of the least-squares minimisation $\tilde{\boldsymbol{q}}_{k+1,m}^*$ is then constrained within prescribed bounds $\boldsymbol{q}_l \leq \tilde{\boldsymbol{q}}_{k+1,m}^* \leq \boldsymbol{q}_u$. Finally, the process noise parameters used to construct the covariance matrix $\tilde{\mathbf{Q}}_{k+1}$ are obtained by applying a smoothing factor α:

$$\tilde{\boldsymbol{q}}_{k+1} = (1-\alpha)\tilde{\boldsymbol{q}}_k + \alpha\tilde{\boldsymbol{q}}_{k+1}^* \quad (7)$$

It is worth noting that the estimated vector $\tilde{q}_{k+1}$, representing the process noise power spectral densities of the empirical accelerations, is used to construct only the submatrix of $\mathbf{Q}$ associated with the satellite dynamical states (position, velocity, and empirical accelerations), following the formulation in [9].

As a result, the adaptive mechanism is applied exclusively to the states related to the spacecraft dynamics. The remaining components of the process noise covariance matrix – namely those associated with clock bias and drift and carrier-phase ambiguities – are kept constant throughout the estimation process.

IV. Simulation Results

A. Scenario and Setup

The developed algorithms have been applied to the TriHex mission concept [12], which has been studied at Politecnico di Milano. TriHex consists of three satellites flying in a fixed triangular configuration along a General Circular Orbit (GCO). The satellites operate in a Sun-Synchronous Orbit at an altitude of 500 km and maintain an inter-satellite baseline of 5 m.

Such a configuration represents a particularly challenging scenario for relative Guidance, Navigation, and Control (GNC), due to the extremely short inter-satellite distances, which impose stringent requirements on relative navigation accuracy and robustness. Although guidance and control strategies for the TriHex formation have been previously investigated [1], studies focusing on the navigation subsystem remain limited.

Therefore, one of the objectives of this work is to assess the feasibility of GNSS-based relative navigation for this class of close formation flying missions. As discussed in Section I, these applications require highly accurate and reliable relative state estimation to ensure safe operation, making the evaluation of advanced filtering techniques particularly relevant.

The initial states for the simulations carried out in this work are reported in Table 1 and Table 2, whereas the initial parameters of the EKF are reported in Table 3. For the clock parameters, the process noise is selected following the theory reported in [10] and based on the type of oscillator.

Table 1. Absolute orbital elements of Virtual (V) Satellite.

Absolute orbital elements	Satellite V
Semimajor axis [km]	6878.1
Eccentricity [-]	0
Inclination [deg]	97.42
Right ascension of ascending node [deg]	8.19
Argument of perigee [deg]	0
Mean anomaly [deg]	0

Table 2. Relative Orbital Elements (ROEs) of formation satellites with respect to Satellite V.

ROEs	Satellite A	Satellite B	Satellite C
$a\delta a$ [m]	0	0	0
$a\delta\lambda$ [m]	0	0	0
$a\delta e_x$ [m]	-0.75	-0.75	1.50
$a\delta e_y$ [m]	-1.30	1.30	0
$a\delta i_x$ [m]	2.25	-2.25	0
$a\delta i_y$ [m]	-1.30	-1.30	2.60

Table 3. EKF Parameters.

Parameter	Value
Process Noise	
σ_N [cycles]	0.1
$\sigma_{N_{\text{SD}}}$ [cycles]	0.05
Measurement standard deviation	
σ_{GR} [m]	0.3
σ_{SDCP} [m]	0.0028

The reference trajectories are generated by numerically propagating the absolute spacecraft states, accounting for a high-fidelity dynamical environment. In particular, the model includes the Earth's gravity field based on the GRACE gravity model up to degree and order 80, atmospheric drag modelled using NRLMSISE-00, third-

body perturbations from the Sun and Moon, solar radiation pressure, and relativistic corrections.
To ensure an accurate assessment of the navigation algorithms, the in-house simulation suite GEMS [13], developed in the MATLAB/Simulink environment, is employed. GEMS is capable of simulating GNSS measurements at the receiver level, providing both pseudorange and carrier-phase observables as outputs representative of onboard measurements.

B. Sensitivity Analysis of Filter Parameters

The performance of both the DMC and, in particular, the ADMC formulations depends on a set of design parameters that must be properly tuned, as they directly influence the filter behaviour.
A parameter common to both the baseline and the adaptive EKF is the autocorrelation time τ associated with the empirical accelerations. In addition, the baseline EKF requires the tuning of the process noise covariance associated with the empirical accelerations. In contrast, in the adaptive formulation, the corresponding parameter is estimated online, and the main tuning parameter becomes the length N of the sliding window used in (4).
To analyse the sensitivity of the filter to these parameters, we first investigate the effect of different initial values of the process noise associated with the empirical accelerations on the performance of both the baseline and the adaptive EKF. The filter performance is assessed by analysing the time evolution of the relative position estimation error, its standard deviation, and the corresponding 1σ confidence level.

Fig. 1 shows the mean values of these quantities for different initial tunings of the process noise, reported in Table 4. A first observation is that the performance of the adaptive filter is independent of the initial choice of process noise covariance. This highlights the capability of the Adaptive EKF (AEKF) to converge to a consistent estimate of the process noise associated with the empirical accelerations, regardless of the initialisation.

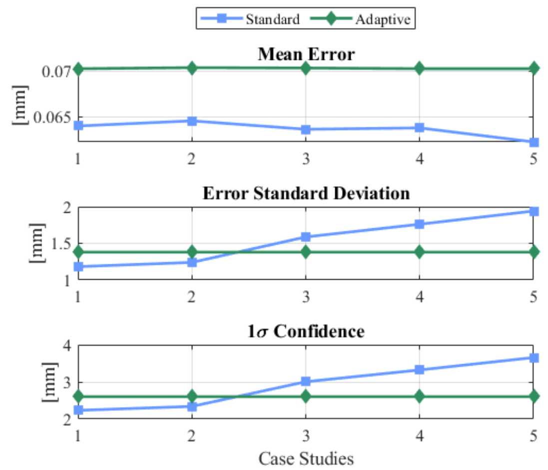

Fig. 1. Results from tuning of process noise of a_{emp}.

Table 4. Initial Process Noise Values.

Case Study	Process Noise in RTN $[\mathrm{nm/s^2}]$
1	$[562.5, 750, 375]$
2	$[750, 1000, 500]$
3	$[3750, 5000, 2500]$
4	$[7500, 10000, 5000]$
5	$[15000, 20000, 10000]$

In contrast, the baseline EKF exhibits a stronger dependence on the selected process noise level. While the mean position error does not show significant variation with respect to the adaptive case, clear trends are observed in the error standard deviation and in the associated 1σ confidence level. In particular, increasing the process noise of the empirical accelerations leads to a corresponding increase in both quantities.
At first glance, these results may suggest that selecting a lower process noise level is preferable in order to achieve higher relative navigation accuracy with the baseline EKF. However, it should be noted that the analysed scenario assumes purely natural orbital motion, with no manoeuvres. Under these conditions, the level of unmodelled dynamics—and thus the process noise associated with the empirical accelerations—is relatively low and does not vary significantly.
In practical applications such as the TriHex mission, a continuous control action is required to maintain the desired formation geometry [1]. This introduces time-varying dynamical effects that may not be adequately captured by a fixed, low process noise setting. In such cases, an underestimation of the process noise associated with the empirical accelerations may lead to degraded performance or filter inconsistency, highlighting the potential benefit of adaptive approaches.
Additionally, it was observed that, for the lower values of process noise associated with the empirical accelerations, the baseline EKF occasionally exhibited poor performance due to inadequate filter convergence. This behaviour was linked to the sensitivity of the filter to the initialisation of the estimated states, which in this study are randomly generated at the start of each simulation run. In particular, insufficient convergence of the filter led to unreliable estimation of the single-difference carrier-phase ambiguities, ultimately resulting in incorrect ambiguity fixing.
This issue was not observed when using the adaptive EKF, which consistently achieved proper convergence and reliable ambiguity resolution, independently of both the initial process noise setting and the initial state conditions. This further highlights the improved robustness of the adaptive formulation with respect to initialisation and modelling uncertainties.

We now analyse the effect of the autocorrelation time τ, defined as the time required for the correlation of the empirical accelerations to decay to 1/e of its initial value.

This parameter influences the performance of both the baseline and the adaptive EKF, as it is not estimated online but must be selected a priori.

In this work, τ is assumed to be identical for all components of the empirical accelerations in the RTN frame, in line with the assumptions adopted in [5]. This represents a simplification, and a more detailed analysis considering different values for each component is left for future work.

Fig. 2 shows the performance of both filters for increasing values of τ. An increase in τ generally leads to an improvement in the estimation performance, as reflected by a reduction in the error standard deviation and in the associated confidence bounds. This behaviour would suggest the selection of relatively large values of the autocorrelation time.

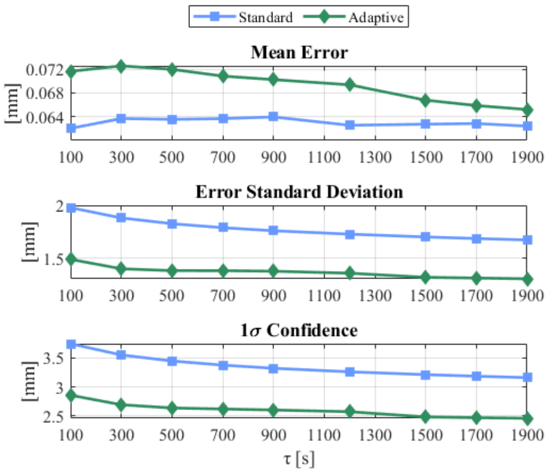

Fig. 2. Results from tuning of τ.

However, since the empirical accelerations are estimated independently for each spacecraft, it is also important to assess the impact of τ on the estimation of the absolute spacecraft states. Fig. 3 shows the standard deviation of the absolute position error for one representative spacecraft, since similar behaviour is observed for the others.

To ensure filter consistency, the value of τ that minimises the standard deviation of the absolute position error is selected, as it represents the best compromise between model fidelity and estimation performance for the considered orbital scenario.

The final parameter considered is the window length N, which is specific to the adaptive filter. The performance of the AEKF for different values of N is shown in Table 5. The results indicate that the filter performance is only mildly sensitive to this parameter, with slightly improved behaviour observed for larger window sizes.

However, increasing N also implies a higher memory requirement, as past data must be stored over the entire window. Therefore, the choice of N represents a trade-off between estimation performance and computational resources and should be selected based on the constraints of the specific application.

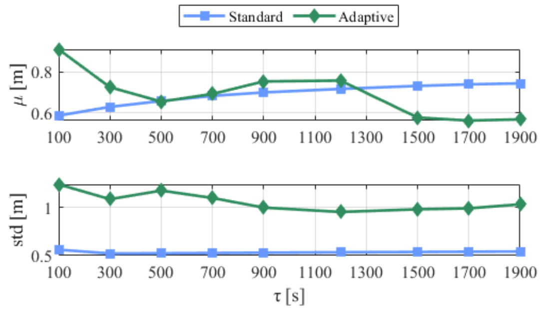

Fig. 3. Statistics of absolute position estimation.

Table 5. Results from tuning N (in [mm]).

N	Mean Error	Std Error	1σ level
10	0.073	1.513	2.864
30	0.067	1.395	2.662
60	0.070	1.380	2.603

C. *Performance Comparison*

This section presents the performance of the baseline EKF and the Adaptive EKF (AEKF) using the parameter values identified through the sensitivity analysis and reported in Table 6. The objective is to evaluate the achievable navigation accuracy under nominal conditions and to assess the impact of the adaptive formulation on the estimation performance.

Table 6. EKF Parameters after sensitivity analysis.

Parameter	Value
$\sigma_{a_{emp}}$ [nm/s^2]	[7500, 10000, 5000]
τ [s]	1500
N [−]	60

Fig. 4 shows the estimation error of the relative state between satellites A and B for the baseline EKF, with the associated statistical indicators reported in Table 7. The corresponding results for the AEKF are presented in Fig. 5 and Table 8.

Table 7. Statistics of relative state estimation (Baseline EKF).

Relative State	Error	1σ level
r_R	-0.02 ± 1.34 mm	2.56 mm
r_T	0.04 ± 0.77 mm	1.52 mm
r_N	0.01 ± 0.53 mm	1.03 mm
v_R	-0.05 ± 42.26 μm/s	101.86 μm/s
v_T	-0.01 ± 31.34 μm/s	79.58 μm/s
v_N	0.07 ± 21.31 μm/s	50.68 μm/s

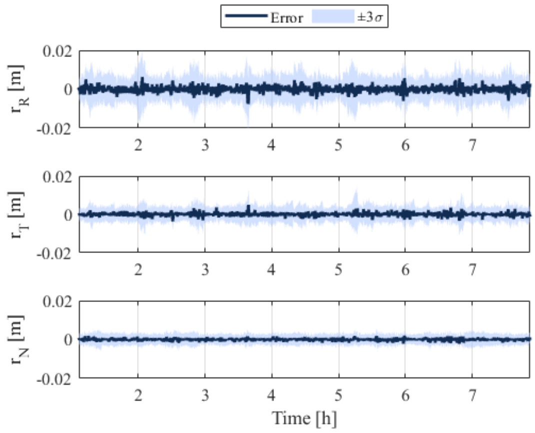

Fig. 4. Relative position estimation error (Baseline EKF).

Table 8. Statistics of relative state estimation (AEKF).

Relative State	Error	1σ level
r_R	-0.03 ± 1.03 mm	1.93 mm
r_T	0.04 ± 0.61 mm	1.21 mm
r_N	0.02 ± 0.46 mm	0.88 mm
v_R	-0.09 ± 20.34 μm/s	43.52 μm/s
v_T	-0.04 ± 16.84 μm/s	42.18 μm/s
v_N	0.09 ± 15.27 μm/s	32.99 μm/s

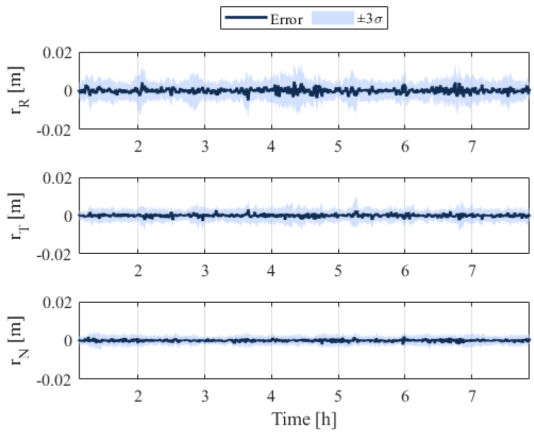

Fig. 5. Relative position estimation error (AEKF).

The results demonstrate that both approaches achieve a level of accuracy at the millimetre scale, representing an improvement with respect to typical GNSS-based relative navigation performance for onboard applications. This is partly enabled by the very short inter-satellite distance, which reduces the impact of common-mode errors in the measurements.

A comparison between the baseline EKF and the AEKF shows that the two filters exhibit very similar performance under nominal conditions, with the AEKF providing a marginal improvement in the considered metrics. This behaviour is influenced by the selected tuning of the process noise associated with the empirical accelerations (see previous section). In particular, adopting lower process noise values would likely improve the performance of the baseline EKF.
However, as discussed in the sensitivity analysis, excessively low values of the process noise may lead to poor filter convergence and unreliable ambiguity resolution, especially under non-ideal conditions. This highlights a criticality of the baseline EKF, which requires careful tuning to balance accuracy and robustness.

Therefore, while the baseline EKF may achieve slightly better performance in ideal conditions with optimally tuned parameters, the AEKF provides a more robust navigation solution. In particular, it is able to maintain consistent performance across a wider range of initial conditions and parameter settings, which is a key advantage for autonomous and safety-critical operations.

V. CONCLUSIONS

This paper presented an investigation of GNSS-based relative navigation for close formation flying missions with metre-level inter-satellite baselines. A baseline EKF was developed to achieve high estimation accuracy, while and adaptive filtering approach based on the ADMC framework was integrated to enhance robustness and autonomy.
The proposed methods were assessed through simulations of the TriHex mission scenario, characterised by a challenging 5 m baseline in LEO. The results demonstrated that real-time GNSS-based techniques can achieve millimetre-level relative positioning accuracy under nominal conditions, confirming their applicability even in very close proximity scenarios.
The comparison between the baseline EKF and the Adaptive EKF showed that, although the baseline formulation can achieve slightly better nominal accuracy when optimally tuned, it is more sensitive to initial conditions and parameter selection, and may suffer from convergence issues. In contrast, the adaptive formulation demonstrated improved robustness, maintaining consistent performance across a wider range of conditions and enabling reliable ambiguity resolution without the need for precise tuning.
These results indicate that adaptive filtering does not necessarily improve nominal accuracy, but provides a significant benefit in terms of robustness and autonomy, which are key requirements for safety-critical close formation flying missions. Future work will extend the analysis to scenarios including manoeuvres, where the advantages of adaptive filtering are expected to become even more significant.

VI. ACKNOWLEDGEMENTS

This work was carried out within the Space It Up!

project funded by the Italian Space Agency (ASI) and the Italian Ministry of University and Research (MUR) under contract No. 2024-5-E.0, CUP No. I53D24000060005.

VII. References

[1] Scala, F. (2022). *Multiple Satellites Formation Flying for Earth Observation Applications in Low Earth Orbits*. PhD thesis, Politecnico di Milano.

[2] D'Amico, S., Ardaens, J. S., & Larsson, R. (2012). Spaceborne autonomous formation-flying experiment on the PRISMA mission. *Journal of Guidance, Control, and Dynamics*, 35(3), 834-850.

[3] Kahr, E., Roth, N., Montenbruck, O., Risi, B., & Zee, R. E. (2018). GPS relative navigation for the CanX-4 and CanX-5 formation-flying nanosatellites. *Journal of Spacecraft and Rockets*, *55*(6), 1545-1558.

[4] Montenbruck, O., Wermuth, M., & Kahle, R. (2011). GPS based relative navigation for the TanDEM-X mission-first flight results. *Navigation*, 58(4), 293-304.

[5] Giralo, V., & D'amico, S. (2019). Distributed multi-GNSS timing and localization for nanosatellites. *Navigation*, *66*(4), 729-746.

[6] Busse, F. D., How, J. P., & Simpson, J. (2003). Demonstration of adaptive extended Kalman filter for low-earth-orbit formation estimation using CDGPS. *Navigation*, *50*(2), 79-93.

[7] Fraser, C. T., & Ulrich, S. (2021). Adaptive extended Kalman filtering strategies for spacecraft formation relative navigation. *Acta Astronautica*, *178*, 700-721.

[8] Stacey, N., & D'Amico, S. (2021). Adaptive and dynamically constrained process noise estimation for orbit determination. *IEEE Transactions on Aerospace and Electronic Systems*, *57*(5), 2920-2937.

[9] Carpenter, J. R., & D'Souza, C. N. (2025), *Navigation Filter Best Practices* (NASA/TP-2018-219822/Revision). National Aeronautics and Space Administration (NASA). [Online]. Available: https://ntrs.nasa.gov/api/citations/20250002787/downloads/20250002787.pdf

[10] Brown, R. G., & Hwang P. Y. C. (2012). *Introduction to Random Signals and Applied Kalman Filtering: With MATLAB Exercises* (4 ed). Wiley & Sons.

[11] Teunnissen, P. J. G. (1995). The Least-Squares Ambiguity Decorrelation Adjustment: A Method for Fast GPS Integer Ambiguity Estimation. *J. Geodesy*, 70(1), 65-82.

[12] Martín-Neira, M., Scala, F., Zurita, A. M., Suess, M., Piera, M., Duesmann, B. J., & Corbella, I. (2023) TriHex: Combining Formation Flying, General Circular Orbits, and Alias-Free Imaging, for High-Resolution L-Band Aperture Synthesis. *IEEE Transactions on Geoscience and Remote Sensing*, 61, 1-17.

[13] Michelazzi, A., Gaias, G., & Colombo, C. (2025). Modelling and Simulation of GNSS Observables for Spacecraft Navigation. *IFAC-PapersOnLine*, 59(31), 67-72.